*Desalination and Water Treatment*
www.deswater.com

doi: 10.5004/dwt.2023.29952

312 (2023) 70–78
November

# Removal of toxic heavy metal ion from tannery effluent by using *Fusarium subglutinans* and *Hylocereus undatus*

A. Latha[a,*], R. Ganesan[b], G. Venkatesan[c], P. Baraneedharan[d]

[a]*Department of Civil Engineering, Panimalar Engineering College, Chennai-123, Tamil Nadu, India, Tel.: +91-9962602435; email: lathaganesan.a@gmail.com, Orchid: http://orchid.org/0000-0003-4784-5732 (A. Latha)*
[b]*Department of Civil Engineering, Saveetha School of Engineering, Saveetha Institute Medical and Technical Sciences (SIMATS), Chennai-105, Tamil Nadu, India, Tel.: +91-9444751780; email: grganeshr4@gmail.com, Orchid: http://orchid.org/0000-0001-8961-7717 (R. Ganesan)*
[c]*Department of Civil Engineering, Saveetha Engineering College, Chennai-105, Tel.: +91-9789290995; email: peccivilvenkat@gmail.com, Orchid: https://orcid.org/0000-0001-8506-6479 (G. Venkatesan)*
[d]*Department of Electronics and Communication Engineering, Saveetha Engineering College, Chennai-602 105, Tamil Nadu, India, Tel.: +91-94436 48262; email: pbaraneedharan@saveetha.ac.in, Orchid: https://orcid.org/0000-0001-8506-6478 (P. Baraneedharan)*

Received 2 April 2023; Accepted 7 September 2023

**ABSTRACT**

The major sources of aquatic pollution are tannery effluent from tannery industries. One of method for removing harmful metals from natural water and commercial refuse sources is biosorption of heavy metals. The chrome tannery wastewater sample was procured from State Industries Promotion Corporation of Tamil Nadu Ltd (SIPCOT). To isolate the metal-tolerant fungus with the ability to absorb heavier metal chromium, the gathered specimens were serially reduced. It offers a possible substitute for the traditional method of eliminating metals. The filtered fungal biomass *Fusarium subglutinans* and agro-waste biosorbent *Hylocereus undatus* are used to remove the $Cr^{6+}$ which is present in tannery effluent. The atomic absorption spectrophotometer was used to ascertain the remaining Cr level in solution. The highest % elimination of $Cr^{6+}$ for the mixed biosorbent was determined to be 98.67% at 50 mg/L starting $Cr^{6+}$ content, 5 g biosorbent dose, pH 2.0, and 150 rpm agitation speed at room temperature. The optimal period for $Cr^{6+}$ biosorption on the biosorbent was 60 min. Finding the biosorption process efficiency requires determining its balance. The equilibrium parameters were examined. The association coefficient ($R^2$) for mixed biosorbent was discovered to be in the following order: Redlich–Peterson (0.9877) > Langmuir (0.8319) > Sips (0.7913) > Freundlich (0.5769). The findings indicated that mixed biosorbent had the capability to remove $Cr^{6+}$, and the amount of $Cr^{6+}$ removed from chrome tannery wastewater was determined to be 99.87%. The elimination of $Cr^{6+}$ from chrome tannery wastewater is a practical, affordable, and environmentally beneficial procedure, according to the analysis of the processed effluent.

*Keywords:* Heavy metal; Dragon fruit peel; Adsorbent dosage; Biosorbent; Kinetic analysis

## 1. Introduction

There are many different ways contaminants can affect our well-being and quality of life, including oxygen, fluids, soil, and the growing commotion we experience [1–3]. The demographic expansion and the consequent increase in destitution are the contributing factors. Urban development, production, the abundance of environmental assets has an impact on the ecosystem in addition to financial growth [4–6]. A vital resource in some areas of the globe is water. According to an article, 80% of humanity is subjected to a danger of an increased degree of water safety [7,8]. Graphite particle (GP) and carbon cloth (CC) are employed as anode electrodes to study both bio-energy generation, and

* Corresponding author.

decrease of chemical oxygen demand simultaneously using tannery effluent. Marine habitats suffer if effluent that has not been purified is released into indigenous aquatic systems [9–11]. This can result in healthcare issues for nearby residents. In the future years, if new methods of supplying pure water are not identified, a lack of water could cause societal and legislative chaos, water disputes, and illnesses [12–14]. Therefore, reducing water contamination leads to fewer water-borne illnesses, increased commercial and farming, marine existence, and fauna. Strong elements in the environment are a major source of concern due to their peril [15–17]. The metals are Cd, Co, Cu, Cr, Pb, Ni, and Zn. These metals are the top contaminants, and because of their high toxicity, they must undergo proper mitigation before being released into the atmosphere. In pure water, the two most common types of Cr are hexavalent chromium [Cr(VI)] and trivalent chromium [Cr(III)]. While soldering on SS or heating chrome metal, the hexavalent Cr can be created [18–20]. Here, the Cr is not hexavalent initially. However, the process's high temperature causes oxidation, which turns the Cr into a hexavalent variant [21–23]. The European Restriction of Hazardous compounds directive prohibits the utilization of including hexavalent chromium [24]. The redox condition and stability of Cr molecules are key determinants of their hazard. In potable and freshwater waterways, the threshold levels for Cr(VI) are 0.05 and 0.1 mg/L, correspondingly [25,26].

## 2. Materials and methods

### 2.1. Fungal biosorbent

The filtered *Fusarium subglutinans* fungal biomass were resuspended in purified water for washing and again filtered as above to make sure that no media remain on the cell surface [27,28]. To eliminate the moisture level, the fungus material was desiccated in a heated air furnace at 100°C for 5 h. In order to handle the Cr(VI) ions, the desiccated fungus sample powder was used as a biosorbent. The fungal biosorbent used in the experiment is shown in Fig. 1.

Fig. 1. Filtered *Fusarium subglutinans* fungal biomass.

### 2.2. Agro-waste as biosorbent

*Hylocereus undatus* (dragon fruit peel) was utilized for the elimination of $Cr^{6+}$ from polluted water as shown in Fig. 2. The refuse from dragon fruit was carefully cleaned with deionized water before being desiccated outside for 24 h [29,30]. The desiccated dragon fruit was dehydrated in a heated ventilation oven at 70°C for 24 h. After that, the desiccated dragon fruit refuse was pulverized and filtered through 100 pores before being kept in plastic containers.

## 3. Characterisation analysis

Several diagnostic methods, including scanning electron microscopy, energy-dispersive X-ray spectroscopy, and Fourier-transform infrared spectroscopy (FTIR) were used in this research to analyze the freshly produced blended biosorbent substance.

### 3.1. Scanning electron microscopy methodology

The microstructures of fungi *F. subglutinans* as well as *H. undatus* were shown in Figs. 3 and 4. Scanning electron microscopy was used to investigate the agricultural waste's roughness and porous composition at various enlargements including 1,000x (50 μm), 5,000x (10 μm), 10,000x (5 μm), 25,000x (20 μm) and 100x (500 μm). The absorption procedure is greatly influenced by exterior properties like hole and interior area [31–33]. According to Figs. 3 and 4, agricultural refuse has big spaces, which will increase their ability for intake in the form of a matrix stratum with a cross-linked system.

### 3.2. Energy-dispersive X-ray analysis

Energy scatter X-ray spectroscopy was utilized to identify the elemental makeup as shown in Figs. 5, 6, and Tables 1 and 2. C and $O_2$ were the two main components in the carbon sphere, as shown in Figs. 5 and 6. These components are important for the adsorption process and could improve the ability to adsorb $Cr^{6+}$ ions.

### 3.3. Fourier-transform infrared spectroscopy analysis

Adsorption is a surface occurrence dependent on the functional group located on the absorbent material's surface. *F. subglutinans* and *H. undatus* were utilized to eliminate $Cr^{6+}$ ions from the solution. The functional groups were detected

Fig. 2. *Hylocereus undatus* biomass.

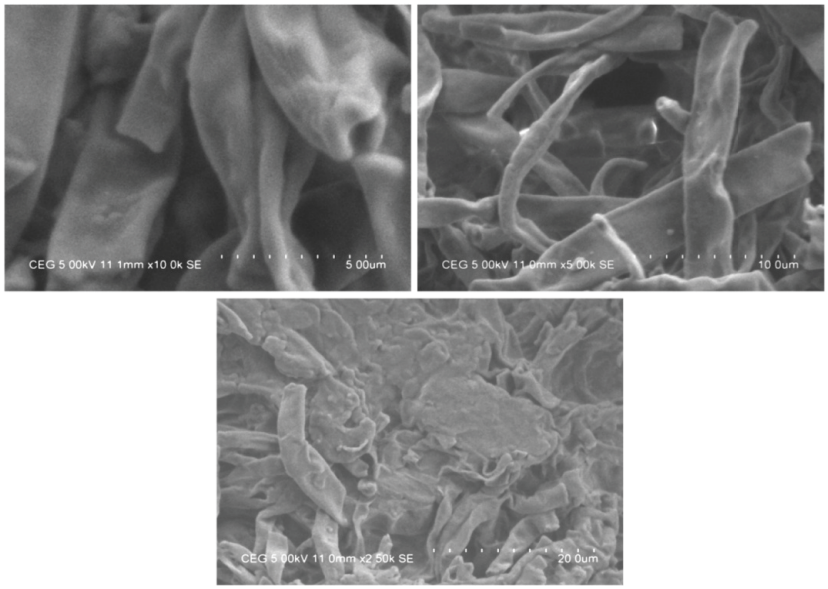


Fig. 3. Scanning electron microscopy images of *Fusarium subglutinans*.

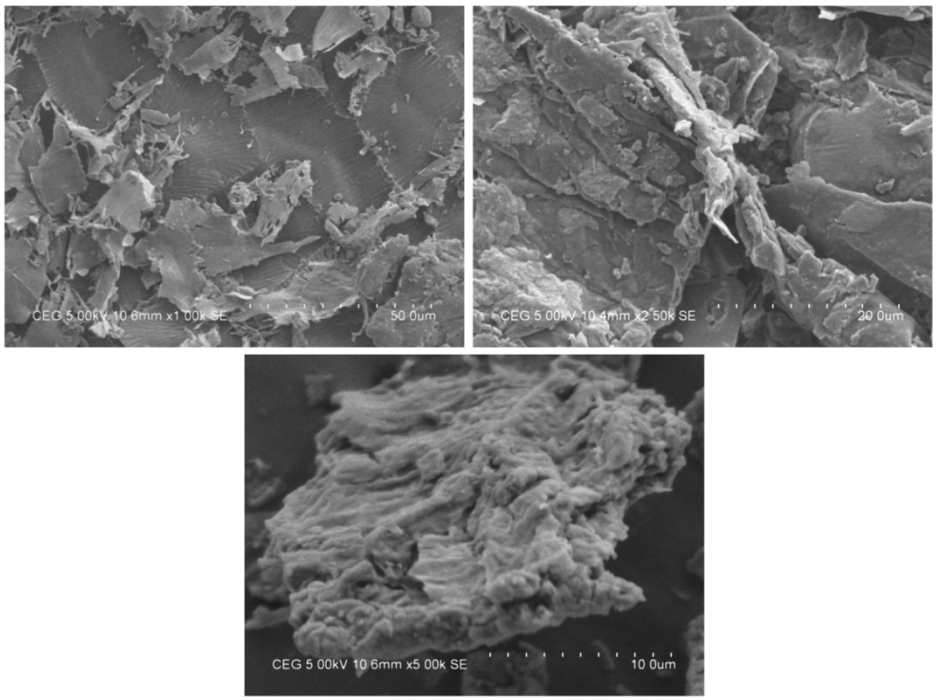


Fig. 4. Scanning electron microscopy images of *Hylocereus undatus*.

using a FTIR spectrophotometer. The attenuated total reflectance in the region of 450–4,000 $cm^{-1}$ was used to examine the images as depicted in Figs. 7, 8, and Tables 3 and 4. The strong signal in Fig. 7 is seen at 3,264 $cm^{-1}$, which is consistent with the existence of a hydroxyl group (O–H linkage). The point at 2,921 $cm^{-1}$ indicates the dominance of methyl C–H twists in the aliphatic groups. The values at 1,622.72 and 1,025 $cm^{-1}$ substantiate the primary amine group frequency of the C–N stretch and alkene group frequency of C=C bends, correspondingly. Fig. 8 shows a strong rise at 3,360.98 $cm^{-1}$, which is consistent with a hydroxyl group (O–H bond). The point at 1,614.22 $cm^{-1}$ denotes C=C twists in the alkene group. The values 1,614.22 and 1,320.59 $cm^{-1}$ correlates with the C=C bending frequency in the alkene and nitro groups, correspondingly. The frequency of the carboxylic acid group as indicated by the absorption point at 1,010 $cm^{-1}$ is the carboxyl C–O stretch. The FTIR analyses substantiated the hydroxyl groups as an important

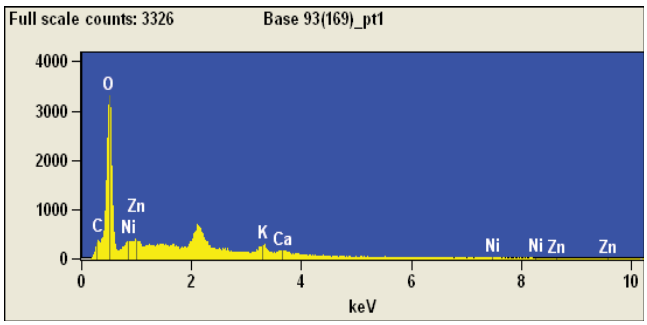


Fig. 5. Energy-dispersive X-ray spectroscopy image of *Hylocereus undatus*.

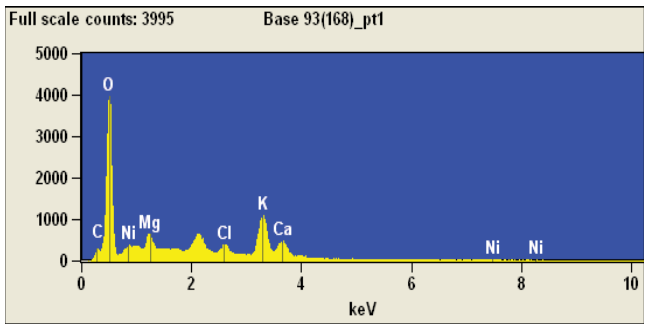


Fig. 6. Energy-dispersive X-ray spectroscopy image of *Fusarium subglutinans*.

Table 1
Energy-dispersive X-ray spectroscopy analysis of *Hylocereus undatus*

| S. No. | Compound | Weight % | Atom % |
|---|---|---|---|
| 1. | Carbon | 9.42 | 12.87 |
| 2. | Oxygen | 81.43 | 83.51 |
| 3. | Potassium | 5.08 | 2.13 |
| 4. | Calcium | 2.86 | 1.17 |
| 5. | Nickel | 0.41 | 0.11 |
| 6. | Zinc | 0.80 | 0.20 |

Table 2
Energy-dispersive X-ray spectroscopy analysis of *Fusarium subglutinans*

| S. No. | Compound | Weight % | Atom % |
|---|---|---|---|
| 1. | Carbon | 3.85 | 5.89 |
| 2. | Oxygen | 70.67 | 81.20 |
| 3. | Magnesium | 3.12 | 2.36 |
| 4. | Chlorine | 2.71 | 1.40 |
| 5. | Potassium | 13.69 | 6.43 |
| 6. | Calcium | 5.82 | 2.67 |
| 7. | Nickel | 0.14 | 0.04 |

component in the formation of covalent bonds. Also, compounds with aliphatic and alkene groupings were initially responsible for the matrix layer development and the cross-linked network between $Cr^{6+}$ ions and binding sites. The produced mixed biosorbent has sufficient capacity for adsorbing $Cr^{6+}$ ions, as revealed by the FTIR measurement.

### 3.4. Adsorption kinetic analysis

Adsorption kinetics was used to demonstrate the adsorption procedure reactivity route and response velocities. The prediction of the sorption process provides crucial information for comprehending the adsorption procedure mechanism which aids in determining the levels at which the $Cr^{6+}$ particles were taken from the water environments. The values rely on how the absorbent materials are described directly. pseudo-first level, pseudo-second level, and the Elovich mechanistic approach were utilized to match the adsorption mechanistic information in order to analyze the sorption rates for the elimination of $Cr^{6+}$ ions utilizing a hybrid adsorbent. The histogram of time ($t$) and $q_t$ were utilized to determine the pseudo-first level kinetic attribute ($k_1$), pseudo-second level kinetic value ($k_2$), equilibrium adsorption potential ($q_e$), the Elovich kinetic model value ($\alpha_E$), and $\beta_E$ values. Using the MATLAB R2009a program, the nonlinear regression analysis was carried out to determine $R^2$, and error values. In Table 5 the computed adsorption kinetic factors and correlation coefficient results ($R^2$) are depicted.

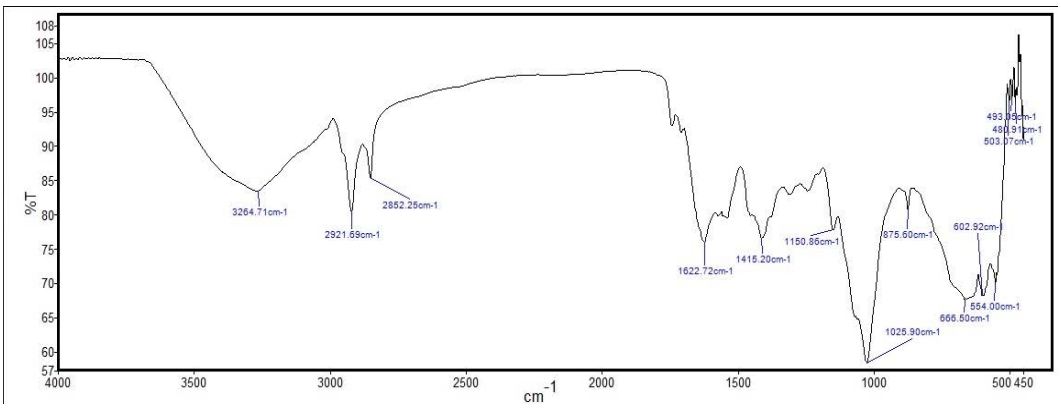


Fig. 7. Fourier-transform infrared spectroscopy image of *Fusarium subglutinans*.

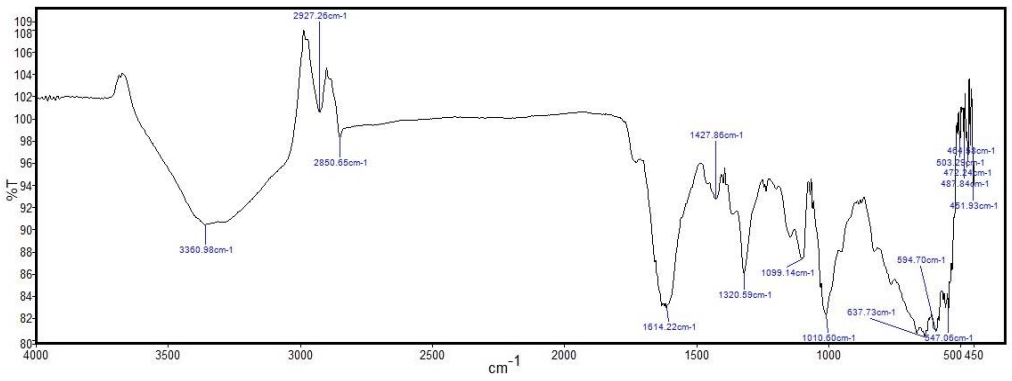


Fig. 8. Fourier-transform infrared spectroscopy image of *Hylocereus undatus*.

Table 3
Fourier-transform infrared spectroscopy analysis of *Fusarium subglutinans*

| Frequency ($cm^{-1}$) | Functional group | Compound |
|---|---|---|
| 3,360.98 | OH | Alcohol |
| 2,927.26 | C–H | Alkanes |
| 2,850.65 | C–H | Alkanes |
| 1,614.22 | C=C | Alkenes |
| 1,320.59 | $NO_2$ | Nitro compound |
| 1,427.86 | C–H | Alkanes |
| 1,099.14 | C–O | Alcohol, ether, esters |
| 1,010.60 | C–F | Aliphatic fluoro compound |
| 637.73 | C–H | Alkynes |
| 594.70 | C–I | Aliphatic iodo compound |
| 547.06 | C–I | Aliphatic iodo compound |
| 503.25 | C–I | Aliphatic iodo compound |
| 487.84 | S–S stretch | Polysulfides |
| 472.24 | S–S stretch | Polysulfides |
| 464.5 | S–S stretch | Aryl disulfides |

Table 4
Fourier-transform infrared spectroscopy analysis of *Hylocereus undatus*

| Frequency ($cm^{-1}$) | Functional group | Compound |
|---|---|---|
| 3,264.71 | O–H | Hydrogen – bonded alcohols, phenols |
| 2,921.69 | C–H | Alkanes |
| 2,852.25 | C–H | Alkanes |
| 1,622.72 | C=C | Alkenes |
| 1,415.20 | C–H | Alkanes |
| 1,150.86 | C–O | Alcohols, ethers, esters, carboxylic acid |
| 1,025.90 | C–N | Primary amine |
| 875.60 | C=C–H (C–H) | Alkenes |
| 666.50 | C–Br | Aliphatic bromo compound |
| 554.00 | C–I | Aliphatic iodo compound |
| 602.92 | C–Br/Disulfides (S–S) | Aliphatic bromo compound |
| 503.07 | C–I | Aliphatic iodo compound |
| 480.91 | S–S | Polysulfides |
| 493.05 | S–S | Polysulfides |

Table 5
Isotherm parameters for $Cr^{6+}$ ion inclusion onto blended biomass

| S. No. | Isotherm model | Variable | $R^2$ | SSE | RMSE |
|---|---|---|---|---|---|
| 1. | Langmuir | $q_m$ (mg/g) = 420.04<br>$K_L$ (L/mg) = 0.4998 | 0.8319 | 2.298 | 53.6 |
| 2. | Freundlich | $n$ = 8.334<br>$K_F$ [(mg/g)(L/mg)$^{(1/n)}$] = 225.1 | 0.5769 | 5.78 | 85.03 |
| 3. | Redlich–Peterson | $\alpha_{RP}$ = 1.89<br>$\beta_{RP}$ = 0.39<br>$K_{RP}$ = 1.928 | 0.9877 | 1.683 | 15.51 |
| 4. | Sips | $\alpha_S$ = 0.13<br>$\beta_S$ = 0.92<br>$K_S$ = 97.7 | 0.7913 | 6.04 | 92.08 |

Three things happened during the inclusion of metal ions onto the porous adsorbents: (1) dispersion of metal ions to the exterior, (2) dissemination openings and (3) metal ions adsorption into inner exterior of the adsorbent. The fundamental formulation can be transformed into a pseudo-first-order formulation at a greater starting quantity of AM or a pseudo-second-order formulation at brief contact times. In the current research, the starting levels of $Cr^{6+}$ ions were comparatively high, and it was discovered that there was little change in concentration during the process. This suggests that the surface adsorption may act as a rate-controlling process, according to the pseudo-first level equation.

## 4. Result and discussions

### *4.1. Effect of original $Cr^{6+}$ ion level*

By changing the $Cr^{6+}$ ion content from 50 to 500 mg/L at pH 2.0, mixed biosorbent quantity of 5 g/L, it was probable to resolve the impact of the original $Cr^{6+}$ ion content on the removal of $Cr^{6+}$ ion using *F. subglutinans* and *H. undatus*. Every collection was stored in a temperature-controlled swaying isolator at 30°C for roughly 60 min, and the outcomes are displayed in Fig. 9. Here, the quantity of $Cr^{6+}$ ions increased from 50 to 500 mg/L and, the elimination dropped from 99.89% to 30.69%. As a set quantity of biosorbent quantity was used for all starting $Cr^{6+}$ ion levels (50–500 mg/L), the available adsorption sites on the mixed biosorbent were submerged. Typically, only the set values of $Cr^{6+}$ particles are removed from the water solution by the specified amount of biosorbent.

### *4.2. Influence of contact duration*

It was possible to ascertain the effect of the initial $Cr^{6+}$ ion level using *F. subglutinans* and *H. undatus* by altering the $Cr^{6+}$ ion level from 50 to 500 mg/L at pH 2.0, blended biosorbent amount of 5 g/L. Every collection was stored in a temperature-controlled swaying isolator at 30°C for roughly 60 min, and the findings are displayed in Fig. 10. Here, the $Cr^{6+}$ ions increased from 50 to 500 mg/L, the elimination dropped from 99.89% to 30.69%. Because only a set quantity of biosorbent was used for all starting $Cr^{6+}$ ion levels (50–500 mg/L), the available adsorption sites on the mixed biosorbent were submerged above a certain percentage of $Cr^{6+}$ ions. Typically, only the $Cr^{6+}$ particles are removed from the water solution by the specified volume of biosorbent.

### *4.3. Effect of pH*

Determining the adsorption procedure is dependent on how the pH of the material influences the electrical contacts among adsorbent and adsorbate. The $Cr^{6+}$ ion solutions at different pH values were set up in order to determine the ideal pH for the inclusion of $Cr^{6+}$ ions and to determine the maximum limit. At either an acidic or a basic pH, the $Cr^{6+}$ particle patterns were weak. The sequential tests were successfully finished in this manner, with a pH between 2.0 to 9.0. The $Cr^{6+}$ ion elimination % is depicted in Fig. 11 for the pH ranges from 2 to 9. Notably, the pH influence was evaluated between 2.0 and 9.0 to prevent chemical formation. This study used a starting $Cr^{6+}$ ion level of 50 mg/L, an interaction duration of 60 min, and an adsorbent dosage of 5 g/L in a solution of 100 mL at 30°C. As the pH rose from 2 to 9, the removal % of $Cr^{6+}$ dropped as seen in Fig. 11. This might be because under highly acidic conditions, an electrical reaction between the negatively charged $Cr^{6+}$ particles and the positively charged biosorbent took place. The excess accessibility of $H^+$ ions cause the functional groups

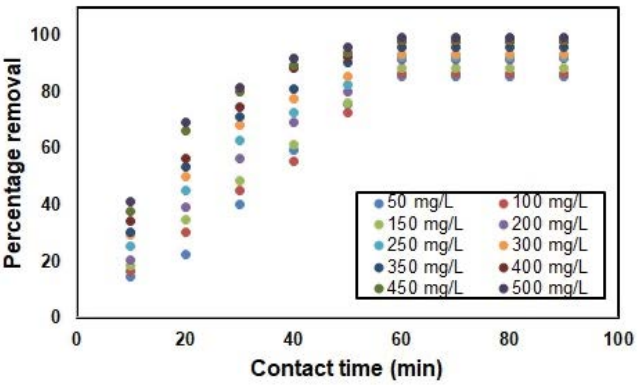


Fig. 10. Effect of interaction time on $Cr^{6+}$ ion deposition onto a blended biosorbent (*Fusarium subglutinans* and *Hylocereus undatus*).

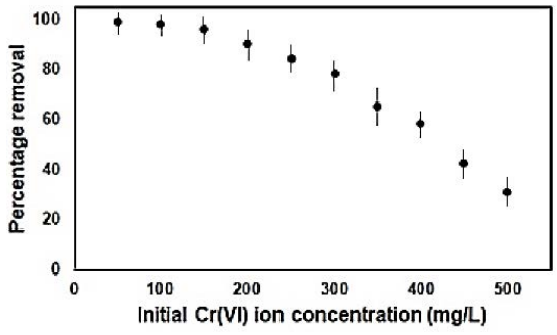


Fig. 9. Impact of $Cr^{6+}$ ion level for the adsorption of $Cr^{6+}$ ions onto the mixed biosorbent (*Fusarium subglutinans* and *Hylocereus undatus*).

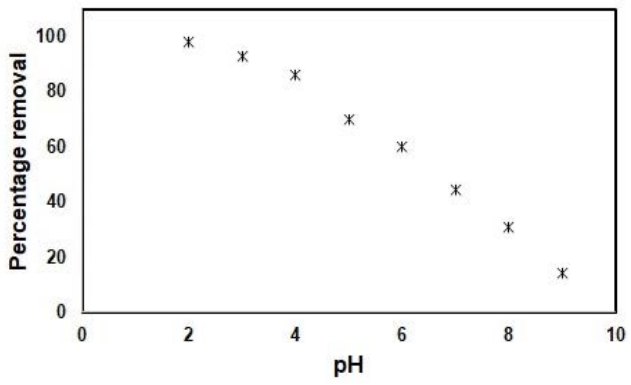


Fig. 11. Influence of pH for the inclusion of $Cr^{6+}$ ions into mixed biosorbent (*Fusarium subglutinans* and *Hylocereus undatus*).

to become protonated at low pH or high acidic pH. When the pH is higher than 2.0, the carbon sphere's exterior has many molecules with net negative charges, repels the $Cr^{6+}$ ions. At pH 9.0, the lowest adsorption limit (LAL) was seen, and at a pH 2.0, the highest adsorption limit (HAL) esteem was observed. It is advised that absorption is supported by electric attraction. At low pH, $Cr^{6+}$ ions are first electrostatically bound to the strongly charged absorbent exterior. After that, the $Cr^{6+}$ anions are slightly altered to Cr(III). Finally, a coordination influence with the lone $N_2$ match electrons causes the Cr(III) particles to become stuck on the absorbent exterior. The research outcome shows that 2.0 is the ideal pH for the greatest elimination of $Cr^{6+}$ ions, suggesting the existence of additional mechanisms, such as physical binding on the sorbent's exterior.

### 4.4. Influence of adsorbent dosage

Adsorbent dose is crucial in the adsorption procedure to assess the material's ability to absorb. At a temperature of 30°C, 100 mL of 50 mg/L $Cr^{6+}$ ion content and a pH of 2.0 in the solution were used to evaluate the biosorbent influence on the elimination of $Cr^{6+}$ ions. According to Fig. 12, the elimination % of $Cr^{6+}$ ions rose as the adsorbent level grew from 1.0 to 8.0 g/L. The reason is due to the presence of additional adsorptive spots on the exterior. The $Cr^{6+}$ elimination was maximized at a dose of 5 g/L. The elimination % of $Cr^{6+}$ was consistent above 5 g/L.

### 4.5. Influence of temperature

The absorption procedure is directly impacted by temperature. At various temps spanning 30°C–60°C and retaining the other factors, the impact of temperature on the absorption of $Cr^{6+}$ by biosorbent was analyzed. According to Fig. 13, the removal % of $Cr^{6+}$ dropped as temperature rose from 30°C to 60°C. This is due to an adhesion forces reduction among the $Cr^{6+}$ and the binding locations on the carbon spheroid's exterior. This demonstrated the current adsorbent device's exothermic character.

### 4.6. Adsorption isotherm analysis

Adsorption isotherm research is a crucial modeling technique that can be utilized in the construction and evaluation of the adsorption mechanism in the adsorption process. The spread of the adsorbate is shown by the adsorption isotherm. $Cr^{6+}$ ion solutions starting concentrations varied from 50 to 500 mg/L. The equilibrium adsorption quantity declined as equilibrium $Cr^{6+}$ ion amounts rose, according to the adsorption isotherm. In this research, the adsorption balance information was described utilizing four adsorption formulations. The parameters inclusive of $K_L$, $q_m$, $K_F$, $K_{RP}$, $\alpha_{RP}$, $\beta_{RP}$, $K_S$, $\alpha_S$ and $\beta_S$ were determined. By using $C_e$ and $q_e$ to draw the curve, the adsorption isotherm parameters, $R^2$, SSE, and RMSE were determined and shown in Fig. 14. According to the compilation summary, the Redlich–Peterson isotherm model (RPIM) had higher $R^2$ values than other isotherm models. The following selection of the top-fitting isotherm models for the current adsorption system was based on $R^2$ values: Peterson, Langmuir, Sips, and Redlich. This suggests that the layered adsorption might be accountable for the absorption of $Cr^{6+}$ ions using mixed biosorbent. The RPIM primarily indicates the adsorbent's surface variability. This demonstrates how the uneven areas on the absorbent surface were perfect. The LM demonstrates that the monolayer adsorption process onto a uniform surface is used in the inclusion of $Cr^{6+}$ ions. The binding between the $Cr^{6+}$ ions and the absorbent can be predicted utilizing the Langmuir inclusion variables. The inclusion strength is better at greater quantities but worse at lower concentrations, according to the Freundlich model. This implies that

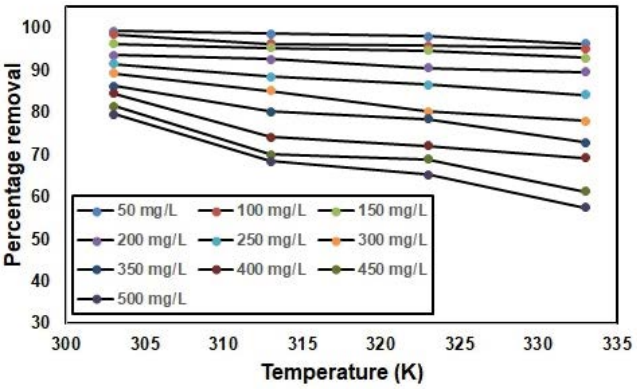


Fig. 13. Influence of temperature for the $Cr^{6+}$ inclusion (*Fusarium subglutinans* and *Hylocereus undatus*).

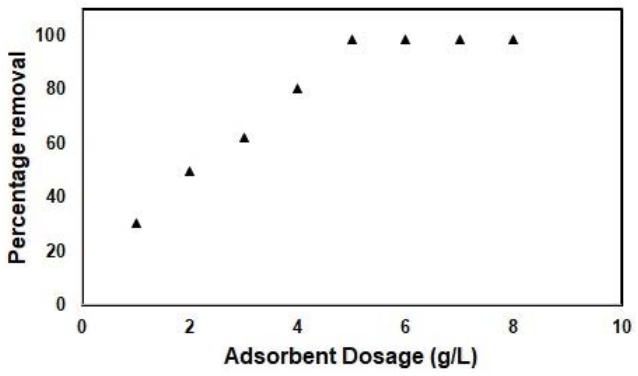


Fig. 12. Influence of adsorbent dosage for $Cr^{6+}$ inclusion (*Fusarium subglutinans* and *Hylocereus undatus*).

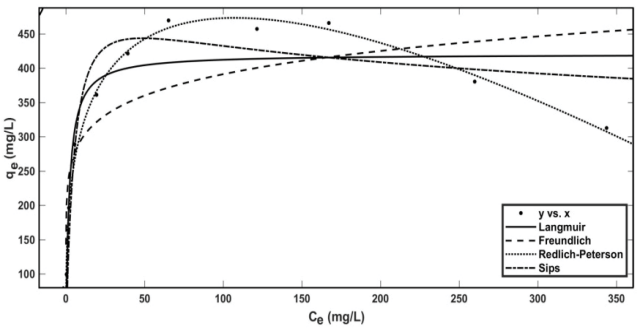


Fig. 14. Adsorption isotherm fit for the adsorption of $Cr^{6+}$ ions into blended biosorbent (*Fusarium subglutinans* and *Hylocereus undatus*).

the absorption surfaces on the adsorbents are diverse. The greatest $K_E$ number for $Cr^{6+}$ ions is an indication of the mixed biosorbent's greater binding capability. $R^2$ numbers were used to discover which models had the greatest potential for fitting the trial data. For mixed biosorbent, the RPM gives high values of $R^2$ (0.9877), and low values of error (1.683 and 15.51). The nonlinear regression technique produces very well-fitting findings and is thought to be more trustworthy.

### 4.7. Adsorption kinetic methodology

Adsorption kinetics was used to elucidate the adsorption process reactivity route and reaction rates. The prediction of the sorption kinetic provides information for comprehending the mechanism of the sorption process as well as calculating the level where the $Cr^{6+}$ were taken from the water solutions. Adsorption levels rely on how the absorbent materials are described physically and/or chemically. Pseudo-first level, pseudo-second level, and the Electro Kinetics (EK) formulation were utilized to match the adsorption mobile information to investigate the adsorption kinetics for the elimination of $Cr^{6+}$. The histogram of time ($t$) and $q_t$ were utilized to determine the pseudo-first level kinetic value ($k_1$), pseudo-second level kinetic value ($k_2$), equilibrium adsorption potential ($q_e$), the EK value ($\alpha_E$), and $\beta_E$ values. Using the MATLAB R2009a program, the methodology was carried out to determine $R^2$, and error values. In Fig. 15 the computed adsorption kinetic factors and correlation coefficient results ($R^2$) are depicted. Three things took place: (1) dispersion of metal ions to the exterior (2) dissemination of metal ions and (3) metal ions adsorption into inner exterior of the adsorbent. The fundamental formulation can be transformed into a pseudo-first-order formulation at a greater starting quantity of AM or a pseudo-second-order formulation at brief contact times. In the current research, the starting levels of $Cr^{6+}$ were comparatively high, and it was discovered that there was little change in concentration during the process. This suggests that the surface adsorption may act as a rate-controlling process, according to the pseudo-first level kinetic formulation. The chemisorption process on the uneven surface is explained by the EK model. With the help of the adsorption kinetic data, the EK equation's non-linear version is verified, and the parameters are assessed. The EK equation is found to support the chemisorption mechanism. The EK model's projected $R^2$ value for the current system was poor. This shows that chemisorption is not the cause of the absorption of $Cr^{6+}$ onto the biosorbent's surface.

### 4.8. Thermodynamic study

$\Delta H°$ and $\Delta S°$ were determined from the slope and intersection of the curve of $\ln K_c$ vs. $1/T$, as shown in Fig. 16, respectively. The values of $\Delta G°$ gradually increased as $T$ rose from 303 to 333 K, hinting that spontaneous inclusion of $Cr^{6+}$ onto the mixed biosorbent was possible. The increase in temperature caused the previously bound $Cr^{6+}$ ions to migrate more freely, which led to a pattern of $Cr^{6+}$ desorption from the biosorbent surface. The following was a summary of the benefits of Gibbs free energy: If the estimated $\Delta G°$ ranges from 20 to 0 kJ/mol, this indicates physical

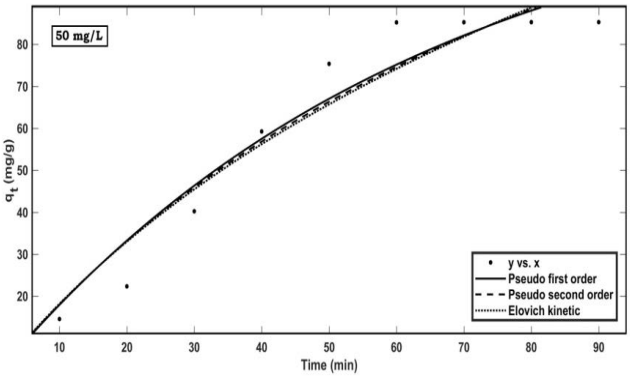


Fig. 15. Adsorption kinetic fit for the inclusion of $Cr^{6+}$ onto combined biosorbent (*Fusarium subglutinans* and *Hylocereus undatus*) $Cr^{6+}$ level = 50 mg/L, contact duration = 60 min, pH = 2.0, adsorbent level = 5 g/L, temperature = 30°C)

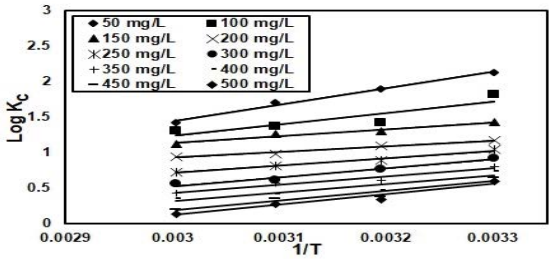


Fig. 16. Thermodynamic study.

absorption. If the estimate of $\Delta G°$ is among 400 and –80 kJ/mol, then that shows synthetic absorption. For the current setup, the $\Delta G°$ values reduced from 20 to 0 kJ/mol for all envisioned temperatures. This indicated that the current inclusion of $Cr^{6+}$ particles onto mixed biosorbent was a substantial adsorption. The exothermic character of the binding of $Cr^{6+}$ ions onto the mixed biosorbent is indicated by the – readings of ($\Delta H°$). Similar to this, the decreased roughness at the solid/fluid contact throughout the procedure was shown by negative values of $\Delta S°$.

## 5. Conclusion

Due to the use of inexpensive sorbing materials, adsorption offers a low-cost alternative to traditional processes when the feedstock being used is refuse. On the other hand, natural approaches provide a chance for the extremely precise elimination of contaminants along with a lot of practical freedom. Numerous of these processes make use of microorganisms that are crucial to the sorption of harmful elements. The ability of different organic components to attach metals forms the foundation for this process. The benefits of biosorption, that utilizes fungus and farming base materials in fermenting and agrarian procedures, include excellent metal elimination efficacy and cost effectiveness. The fungus sample was then mass-cultured, desiccated, and ground to remove the $Cr^{6+}$. Then, it was blended with the pulverized *H. undatus* resulting in the mixed biosorbent. To effectively address the issue of

heavy metal contamination release from businesses, a biosorption trial was conducted using actual tannery wastewater and biosorbents (*F. subglutinans* and *H. undatus*). The findings indicated that mixed biosorbent had the capability to remove $Cr^{6+}$, and the amount of $Cr^{6+}$ removed from chrome tannery wastewater was determined to be 99.87%. The elimination of $Cr^{6+}$ from chrome tannery wastewater is a practical, affordable, and environmentally beneficial procedure, according to the analysis of the processed effluent.

## References


[1] M.G. Motitswe, K.O. Badmus, L. Khotseng, Development of adsorptive materials for selective removal of toxic metals in wastewater: a review, Catalysts, 12 (2022) 1057, doi: 10.3390/catal12091057.

[2] N.A.A. Qasem, R.H. Mohammed, D.U. Lawal, Removal of heavy metal ions from wastewater: a comprehensive and critical review, npj Clean Water, 4 (2021) 36, doi: 10.1038/s41545-021-00127-0.

[3] P. Angelin Vinodhini, P.N. Sudha, Removal of heavy metal chromium from tannery effluent using ultrafiltration membrane, Text. Clothing Sustainability, 2 (2017) 5, doi: 10.1186/s40689-016-0016-3.

[4] Md. Nur-E-Alam, Md. Abu Sayid Mia, F. Ahmad, Md. Mafizur Rahman, An overview of chromium removal techniques from tannery effluent, Appl. Water Sci., 10 (2020) 205.

[5] E.-S.R.E. Hassan, M. Rostom, F.E. Farghaly, M.A. Abdel Khalek, Bio-sorption for tannery effluent treatment using eggshell wastes; kinetics, isotherm and thermodynamic study, Egypt. J. Pet., 29 (2020) 273–278.

[6] A. Shukla, Z. Mahmood, L.K. Singh, Studies on recovery of heavy metals from tannery wastewater, Int. J. Eng. Sci. Technol., 13 (2021) 76–80.

[7] M.A. Renu, K. Singh, Heavy metal removal from wastewater using various adsorbents: a review, J. Water Reuse Desal., 7 (2017) 387–419.

[8] M.R. Shaibur, F.K. Sayema Tanzia, S. Nishi, N. Nahar, S. Parvin, T.A. Adjadeh, Removal of Cr(VI) and Cu(II) from tannery effluent with water hyacinth and arum shoot powders: a study from Jashore, Bangladesh, J. Hazard. Mater. Adv., 7 (2022) 100102, doi: 10.1016/j.hazadv.2022.100102.

[9] K. Aftab, K. Akhtar, A. Kausar, S. Khaliq, N. Nisar, H. Umbreen, M. Iqbal, Fungal strains isolation, identification and application for the recovery of Zn(II) ions, J. Photochem. Photobiol., B, 175 (2017) 282–290.

[10] N. Ahalya, T.V. Ramachandra, R.D. Kanamadi, Biosorption of heavy metals, Res. J. Chem. Environ., 7 (2003) 71–78.

[11] A. Mishra, A. Malik, Novel fungal consortium for bioremediation of metals and dyes from mixed waste stream, Bioresour. Technol., 171 (2014) 217–226.

[12] Y. Sağ, Biosorption of heavy metals by fungal biomass and modeling of fungal biosorption: a review, Sep. Purif. Methods, 30 (2001) 1–48.

[13] S. Smiley, P. Malaviya, Bioremediation of tannery wastewater by chromium resistant novel fungal consortium, Ecol. Eng., 91 (2016) 419–425.

[14] T.G. Chuah, A. Jumasiah, I. Azni, S. Katayon, S.Y. Thomas Choong, Rice husk as a potentially low-cost biosorbent for heavy metal and dye removal: an overview, Desalination, 175 (2005) 305–316.

[15] M. Naveenkumar, K. Senthilkumar, V. Sampathkumar, S. Anandakumar, B. Thazeem, Bio-energy generation and treatment of tannery effluent using microbial fuel cell, Chemosphere, 287 (2022) 132090, doi: 10.1016/j.chemosphere.2021.132090.

[16] O.T. Hoang Le, L.N. Tran, V.T. Doan, Q.V. Pham, A.V. Ngo, H.H. Nguyen, Mucilage extracted from dragon fruit peel (*Hylocereus undatus*) as flocculant for treatment of dye wastewater by coagulation and flocculation process, Int. J. Polym. Sci., 2020 (2020) 7468343, doi: 10.1155/2020/7468343.

[17] M. Kavisri, M. Abraham, S. Karthik Raja Namasivayam, J. Aravindkumar, D. Balaji, R. Sathishkumar, S. Sigamani, R. Srinivasan, M. Moovendhan, Adsorption isotherm, kinetics and response surface methodology optimization of cadmium (Cd) removal from aqueous solution by chitosan biopolymers from cephalopod waste, J. Environ. Manage., 335 (2023) 117484, doi: 10.1016/j.jenvman.2023.117484.

[18] R. Dineshkumar, M. Sowndariya, S. Kalaiselvi, G. Israth Rehana, M. Durai Murugan, M. Abraham, M. Moovendhan, M. Kavisri, Effective removal of lead (Pb) by natural biosorbent marine microalgae (*Dunaliella salina*) through batch experiment, Biomass Convers. Biorefin., (2022), doi: 10.1007/s13399-021-02260-9.

[19] A. Latha, R. Ganesan, L. Karthick, L. Vadivukarasi, Experimental investigation on treatment of textile dyeing effluent by novel electro-Fenton process integrated with laboratory-scale aanaerobic sequencing batch reactor, Biomass Convers. Biorefin., (2023), doi: 10.1007/s13399-023-04524-y.

[20] A. Latha, R. Ganesan, B. Krisnakumari, S. Theerkadarsin, Comparative study of organic coagulants in water treatment, ECS Trans., 107 (2022) 7997, doi: 10.1149/10701.7997ecst.

[21] A. Latha, P. Partheeban, R. Ganesan, Degradation of reactive dyes in textile dyeing effluent by Fenton and electro Fenton processes, Ecol. Environ. Conserv. Paper, EM Int., 24 (2018) 1748–1753.

[22] R. Ganesan, K. Thanasekaran, Degradation of textile dyeing wastewater by a modified solar photo-Fenton process using steel scrap/$H_2O_2$, CLEAN-Soil Air Water, 41 (2013) 267–274.

[23] S.H. Lin, C.F. Peng, Treatment of textile wastewater by electrochemical method, Water Res., 28 (1994) 277–282.

[24] E. Pavithra Krishnan, R. Ganesan, Comparative studies on colour and COD removal of reactive dyes by a novel steel scrap as a catalyst with conventional Fenton process, Revista Gestão Inovação e Tecnologias, 11 (2021) 1264–1276.

[25] G. Venkatesan, T. Subramani, Reduction of hexavalent chromium to trivalent chromium from tannery effluent using bacterial biomass, Indian J. Geo-Mar. Sci., 48 (2019) 528–534.

[26] G. Venkatesan, T. Subramani, Environmental degradation due to the industrial wastewater discharge in Vellore District, Tamil Nadu, India, Indian J. Geo-Mar. Sci., 47 (2018) 2255–2259.

[27] D. Karunanidhi, P. Aravinthasamy, T. Subramani, D. Kumar, G. Venkatesan, Chromium contamination in groundwater and Sobol sensitivity model based human health risk evaluation from leather tanning industrial region of South India, Environ. Res., 199 (2021) 111238, doi: 10.1016/j.envres.2021.111238.

[28] G. Venkatesan, S. Joyal Isac, G. Jerome Nithin Gladson, S. Amala, Demarcation of non-carcinogenic risk zones based on the intake of contaminated groundwater in an industrial area of southern India using geospatial technique, Desal. Water Treat., 274 (2022) 140–149.

[29] D. Sivakumar, V. Balasundaram, G. Venkatesan, S.P. Saravanan, Effect of tamarind kernel powder for treating dairy industry wastewater, Pollut. Res., 33 (2014) 519–523.

[30] G. Venkatesan, M. Kalpana, S. Jegadeesh, B. Praveen, Environmentally-friendly bio-coagulants: a cost-effective solution for groundwater pollution treatment, Asian J. Water Environ. Pollut., 20 (2023) 19–28.

[31] A. Aishwarya Lakshmi, S. Amalraj, G. Venkatesan, Granules as precursors in the working of upflow anaerobic sludge blanket reactor: a review on the impacts of granulation, Asian J. Water Environ. Pollut., 20 (2023) 41–45.

[32] G. Venkatesan, M. Kalpana, S. Sakthivel, K. Guruchandran, W. Mathew, A combined approach for the treatment of textile dye bath effluent using $CO_2$ gas, Asian J. Water Environ. Pollut., 20 (2023) 59–65.

[33] G. Venkatesan, M. Kuberan, B. Praveen, S. Jegadeesh, Treatment of dairy wastewater and sludge production using algae bioreactor, Asian J. Water Environ. Pollut., 20 (2023) 77–83.